



HAL
open science

Neutronic Analysis of the European Sodium Fast Reactor: Part I-Fresh Core Results

Emil Fridman, Francisco Álvarez Velarde, Pablo Romojaro Otero, Haileyesus Tsige-Tamirat, Antonio Jiménez Carrascosa, Nuria García Herranz, Franck Bernard, Robert Gregg, Una Davies, Jiri Krepel, et al.

► **To cite this version:**

Emil Fridman, Francisco Álvarez Velarde, Pablo Romojaro Otero, Haileyesus Tsige-Tamirat, Antonio Jiménez Carrascosa, et al.. Neutronic Analysis of the European Sodium Fast Reactor: Part I-Fresh Core Results. *Journal of Nuclear Engineering and Radiation Science*, 2021, 8 (1), pp.11301. 10.1115/1.4048905 . irsn-04122162v3

HAL Id: irsn-04122162

<https://irsn.hal.science/irsn-04122162v3>

Submitted on 11 Aug 2023

HAL is a multi-disciplinary open access archive for the deposit and dissemination of scientific research documents, whether they are published or not. The documents may come from teaching and research institutions in France or abroad, or from public or private research centers.

L'archive ouverte pluridisciplinaire **HAL**, est destinée au dépôt et à la diffusion de documents scientifiques de niveau recherche, publiés ou non, émanant des établissements d'enseignement et de recherche français ou étrangers, des laboratoires publics ou privés.



Distributed under a Creative Commons Attribution 4.0 International License

Neutronic analysis of the European Sodium Fast Reactor:

Part I - fresh core results

Emil FRIDMAN

Helmholtz-Zentrum Dresden-Rossendorf (HZDR)
Bautzner Landstraße 400, 01328 Dresden, Germany
e.fridman@hzdr.de

Francisco ÁLVAREZ VELARDE

CIEMAT
Av. Complutense, 40, 28040 Madrid, Spain
francisco.alvarez@ciemat.es

Pablo ROMOJARO OTERO

CIEMAT (currently at SCK·CEN)
Av. Complutense, 40, 28040 Madrid, Spain
Pablo.Romojaro@sckcen.be

Haileyesus TSIGE-TAMIRAT

European Commission / Joint Research Centre Petten
Westerduinweg 3. 1755LE Petten
Haileyesus.TSIGE-TAMIRAT@ec.europa.eu

Antonio JIMÉNEZ CARRASCOSA

Universidad Politécnica de Madrid (UPM)
José Gutiérrez Abascal, 2, 28006 Madrid, Spain
antonio.jcarrascosa@upm.es

Nuria GARCÍA HERRANZ

Universidad Politécnica de Madrid (UPM)
José Gutiérrez Abascal, 2, 28006 Madrid, Spain
nuria.garcia.herranz@upm.es

Franck BERNARD

Institut de Radioprotection et Sûreté Nucléaire (IRSN)
31 Avenue de la Division Leclerc, 92260 Fontenay-aux-Roses, France
franck.bernard@irsn.fr

Robert GREGG

National Nuclear Laboratory (NNL)
Chadwick House, Warrington WA3 6AE, UK
robert.wh.gregg@nnl.co.uk

Una DAVIES

University of Cambridge
Trumpington St, Cambridge CB2 1PZ, UK
ud215@hermes.cam.ac.uk

Jiri KREPEL

Paul Scherrer Institut (PSI)
5232 Villigen, Switzerland
jiri.krepel@psi.ch

Simone MASSARA

EDF-R&D, EDF Lab Paris-Saclay (Currently at IAEA)
7 Boulevard Gaspard Monge, 91120 Palaiseau, France
simone.massara@edf.fr (S.Massara@iaea.org)

Sandra POUmeroULY

EDF-R&D, EDF Lab Paris-Saclay
7 Boulevard Gaspard Monge, 91120 Palaiseau, France
sandra.poumerouly@edf.fr

Enrico GIRARDI

EDF-R&D, EDF Lab Paris-Saclay
7 Boulevard Gaspard Monge, 91120 Palaiseau, France
enrico.girardi@edf.fr

Konstantin MIKITYUK

Paul Scherrer Institut (PSI)
5232 Villigen, Switzerland
konstantin.mikityuk@psi.ch

Abstract

In the framework of the Horizon 2020 project ESFR-SMART (2017-2021), the European Sodium Fast Reactor (ESFR) core was updated through a safety-related modification and optimization of the core design from the earlier FP7 CP-ESFR project (2009-2013).

This study is dedicated to neutronic analyses of the improved ESFR core design. The conducted work is reported in two parts. Part I deals with the evaluation of the safety-related neutronic parameters of the fresh Beginning-of-Life (BOL) core carried out by 8 organizations using both continuous energy Monte Carlo and deterministic computer codes. In addition to the neutronics characterization of the core, a special emphasis was put on the calibration and verification of the computational tools involved in the analyses.

Part II is devoted to once-through and realistic batch-wise burnup calculations aiming at the establishing of the equilibrium core state, which will later serve as a basis for detailed safety analyses.

1. Introduction

The Horizon 2020 ESFR-SMART (European Sodium Fast Reactor Safety Measures Assessment and Research Tools) is a four-year collaborative project co-funded by the European Commission within the Euratom research and training programme [1]. The project was launched to enhance further the safety of the commercial-size European Sodium Fast Reactor (ESFR) investigated within the earlier CP-ESFR project [2].

At the initial stage of the project, the modified ESFR core design was obtained through the two-step optimization procedure applied to the SFR core developed within the CP-ESFR project. The new ESFR core design was established by optimizing neutronic, thermal-hydraulic, and fuel performance using multi-physics and multi-objective optimization. The corresponding activities are described in details in the current special issue on ESFR-SMART [3]. Some preliminary information is also available in [4]. The core design modifications were aimed at improving the core map symmetry, optimizing the void effect, and facilitating the corium relocation toward the corium catcher. In addition, the core design aimed at achieving low reactivity swing in connection with a flexible breeding and minor actinide burning strategy.

The main objective of the current study is a neutronic characterization of the new ESFR core. The conducted work is reported in two parts:

- Part I is focused on the evaluation of safety-related neutronic parameters for the fresh core, which are used to calibrate and verify the computer codes used in the analyses.
- Part II is devoted to once-through and realistic batch-wise burnup analysis aimed at establishing the equilibrium core loading pattern [5].

Part I of the paper is structured as follows. Section 2 provides a brief overview of the initial ESFR core. Section 3 discusses the modeling assumptions. Results are presented in Section 4. Section 5 summarizes the paper.

2. A brief description of the initial ESFR-SMART core

This section provides a brief description of the new ESFR core and summarizes the major parameters and the modelling assumptions. The radial core layout is shown in Figure 1. The core consists of inner fuel (IF) and outer fuel (OF) regions loaded with 216 and 288 fuel sub-assemblies (SA) respectively. In the initial core, the Pu content in both zones is identical and equal to 17.99 wt%. Both regions are managed using a 6-batch fuel loading pattern. The core is controlled by 24 control and shutdown devices (CSD) and 12 diverse shutdown devices (DSD). Compared to the SFR core from the CP-ESFR project, new corium discharge tubes (CDT) were introduced into several locations (31 in total) including the central position, the boundary between IF and OF regions, and the core periphery. The active core is surrounded by 3 rings of reflector SA, 2 rings of internal spent fuel storage positions, and 4 rings of shielding SA. Preliminary analysis, performed at CIEMAT, showed a negligible effect of the

spent fuel storage and shielding on neutronics. Therefore, these regions were not considered in the neutronic analyses of the ESRF-SMART core.

The axial layout of the IF and OF SAs is presented in Figure 2. Compared to the initial SFR core from the CP-SFR project, a large sodium plenum followed by a neutron absorber was introduced above the active core. In addition, the heights of the fissile regions were reduced and fertile and steel blankets introduced below. A single fissile enrichment was adopted for both IF and OF regions. In order to improve radial power uniformity, the height of the IF fissile region was further reduced. At room temperature, the active core height is 1 m. The height of the blanket in IF and OF zones is 5 and 25 cm respectively. The height of the sodium plenum is 60 cm. The fissile pellet features an inner hole. The fertile pellet has the same radius as the fuel but no inner hole and a different isotopic composition.

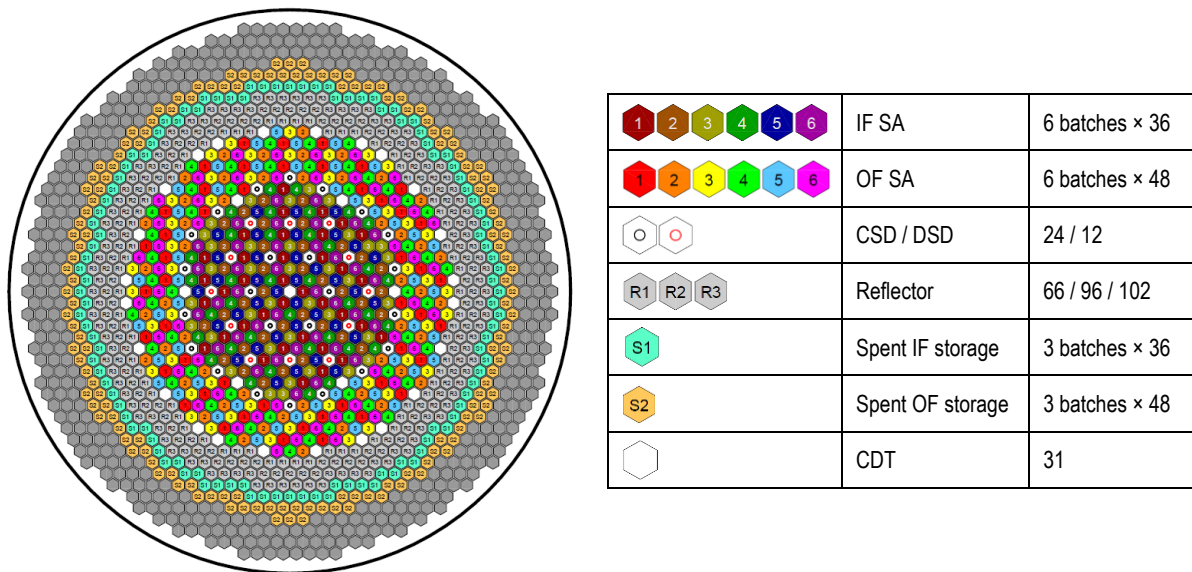


Fig. 1 Radial core layout

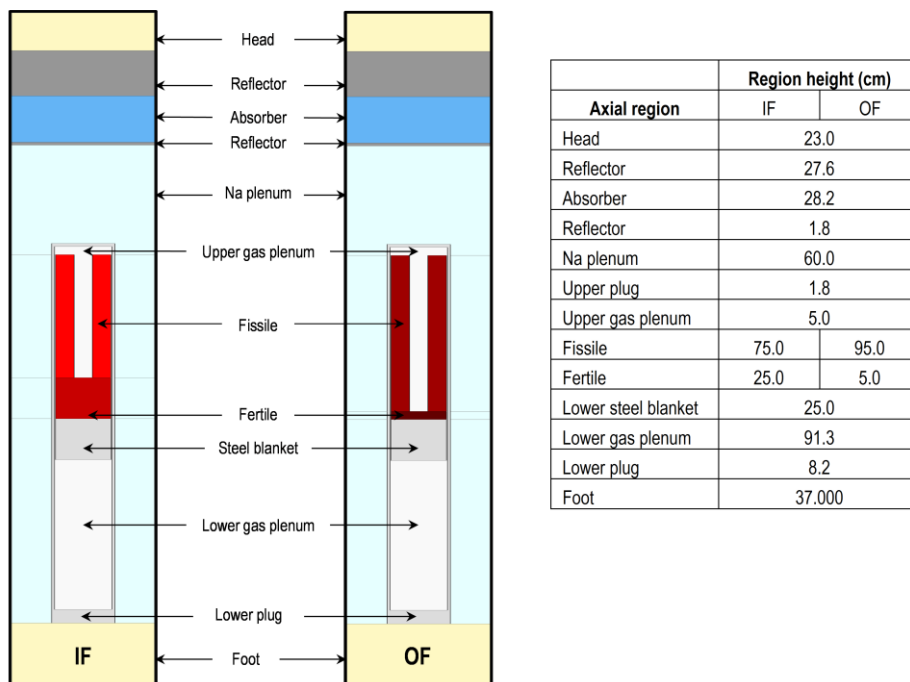


Fig. 2 Axial core layout

3. Modeling assumptions

The neutronic calculations were performed assuming material-uniform temperatures. The adopted temperature values are summarized in Table 1.

Table 1. Nominal material temperatures

Material	Temperature, K
Fissile	1500
Fertile	900
Sodium	900
Core structures	900

The neutronic characterization of the fresh ESRF-SMART core started with the evaluation of the following parameters:

- Core reactivity (ρ) at nominal operating conditions
- SCRAM reactivity
- Sodium void reactivity
- Doppler constants (KD)

The SCRAM reactivity was calculated as a difference in reactivity between the nominal and the fully rodded states. At the nominal state, all CSDs and DSDs are withdrawn to the parking position, that is, the bottom of the control rod is aligned with the top of the upper gas plenum (Figure 2). At the fully rodded state, all CSDs and DSDs are inserted in a way that the bottom of the control rod is aligned with the top of the OF fertile region.

Sodium void reactivity was calculated as a difference in reactivity between the nominal and the voided states. Five voiding scenarios were considered as depicted in Figure 3:

- Void 1: voiding of inner fissile region
- Void 2: voiding of outer fissile region
- Void 3: voiding of everything above inner fissile region
- Void 4: voiding of everything above outer fissile region
- Void 5: voiding of inner and outer fissile region + everything above

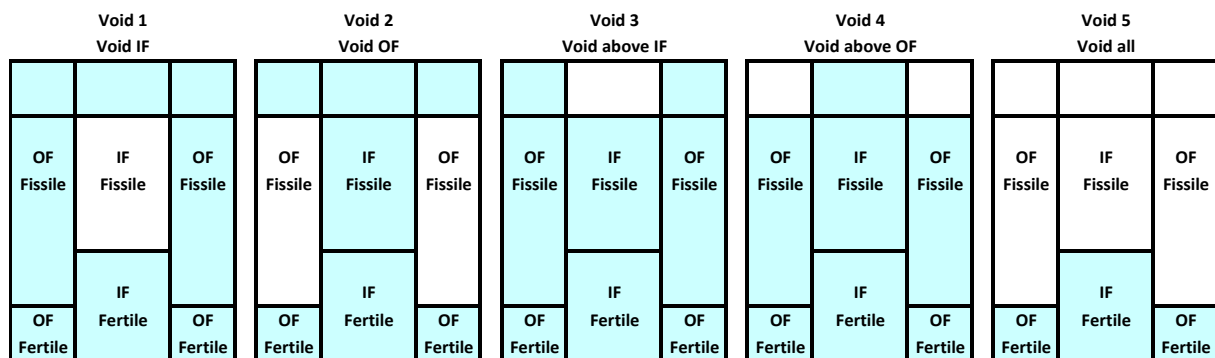


Fig. 3 Considered voiding scenarios

It should be noted that in all voiding scenarios, inter assembly gap was not voided as shown in Figure 4.

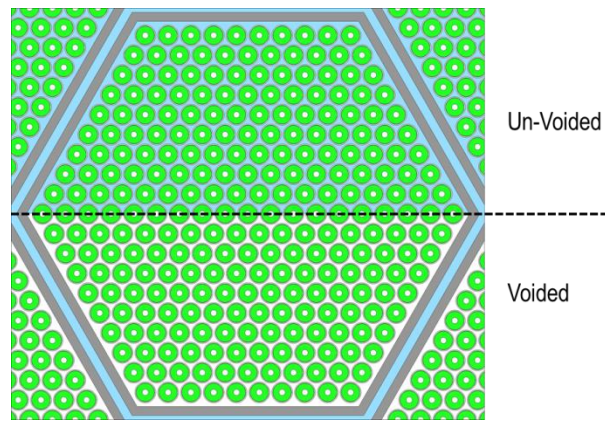


Fig. 4 Approach to the voiding modeling. Inter assembly gap is not voided

Doppler constants of the fissile and fertile regions were estimated using the temperature variations shown in Table 2.

Table 2. Temperature variations for KD calculations

Case	T fissile, K	T fertile, K
KD1	1200	900
KD2	1800	900
KD3	1500	600
KD4	1500	1200

The calculations were carried out by 8 organizations using both continuous energy (CE) Monte Carlo (MC) and deterministic codes. All organizations, except NNL, used the Joint Evaluated Fission and Fusion (JEFF) Nuclear Data library version 3.1 (JEFF3.1) [6], which was thus considered the “default” nuclear data library. A list of contributing organizations, computer codes applied, and nuclear data libraries used is shown in Table 3. The modeling approaches applied are presented below.

Table 3. Participants and codes applied for the characterization of the fresh ESRF core

Organization	Code	Solver	Nuclear data library
HZDR	Serpent 2.1.29 [7]	CE-MC	JEFF-3.1
CIEMAT	MCNP6.1.1b [8]	CE-MC	JEFF-3.1
JRC	MCNP6.1.0 [9]	CE-MC	JEFF-3.1
IRSN	MORET 5.C.1 [10]	CE-MC	JEFF-3.1
UPM	KENO-VI [11]	CE-MC*	JEFF-3.1
NNL/Cambridge	WIMS11 [12]	Deterministic	JEFF 3.1.2
PSI	ERANOS/VARIANT [13]	Deterministic	JEFF-3.1
EDF	ERANOS/VARIANT [13]	Deterministic	JEFF-3.1

*No p-tables in the unresolved resonance region

3.1 MC codes

All MC codes performed direct full core calculations using 3D heterogeneous geometry models and continuous energy nuclear cross section data. The MC models reproduce the heterogeneous geometry fully resolved in both radial and axial direction as given in the ESRF-SMART core specification. The repeated structure feature of the MC codes enables to set up the geometry of the SAs and the full core in an efficient manner.

In the MC criticality calculations, sufficient numbers of neutrons and cycles were considered so that overall adequate statistical uncertainties were achieved. For the evaluation of the core neutronic parameters, the direct eigenvalue method has been used. The method determines core neutronic parameters using eigenvalues calculated for different core configurations with altered characteristics.

3.2 WIMS11

The WIMS code [12] follows a typical two-step approach where the generation of homogenized few-group cross sections is followed by full core calculations. The few-group cross sections were prepared using the following procedure:

- For the fuel cell, an initial flux solution was prepared using WIMS-ECCO and the reference calculation scheme (heterogeneous geometry, initial steps solved using 1968 energy groups, which are then condensed culminating in 172 group data). This was then fed into a 172-group, heterogeneous 2D-MOC solution using CACTUS (a module within WIMS), the results from which were used in the whole core model. Note the central annular hole was modelled explicitly.
- For the fertile cell, a 172-group critical flux spectrum was calculated using ECCO and a homogenous representation of the fissile fuel assembly cell. This driving flux was used in an ECCO model of the fertile fuel cell using the same reference calculation scheme as before. The 172-group flux estimate was then used in a heterogeneous 2D method of characteristics (MOC) solution using CACTUS, the results from which were used in the whole core model.
- All other (structural) cell types were modelled homogeneously in ECCO using the same driving flux from a homogenous representation of the fissile fuel assembly cell. The default subcritical calculation scheme was used (homogenous, initial steps solved using 1968 energy groups, which were then condensed culminating in 172 group data).

In addition, cross sections for the CSD and DSD cells were prepared using a 2D-MOC method (CACTUS) to model a heterogeneous and homogenous representation. A super-homogenization (SPH) method [14] was then used to calculate a set of homogenized equivalent cross-sections thus enabling the reaction rates in the heterogeneous model to be reproduced in the homogenized model. The control rod worths were calculated twice, using both the homogenous and SPH methods.

Finally, the full core calculations were performed as follows:

- 172 group cross section data from the previous ECCO/CACTUS calculations were used in a R-Z model using MERLIN.
- The 172 group data from the previous step was condensed to 33 groups and by MERLIN to model a HEX-Z representation of the core. Flux was solved using the SP3 approximation with vacuum boundary conditions.

3.3 ERANOS

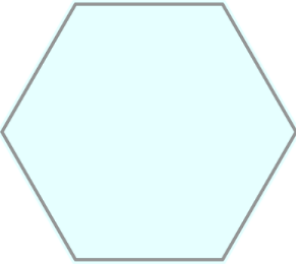
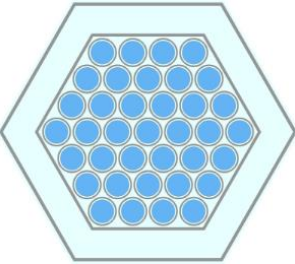
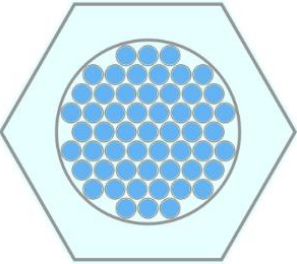
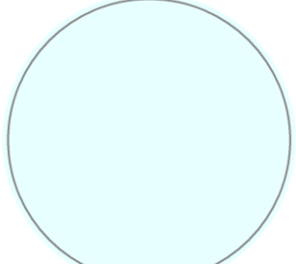
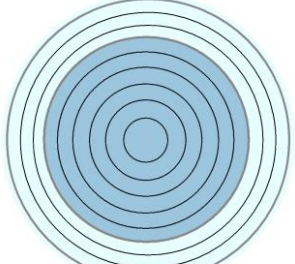
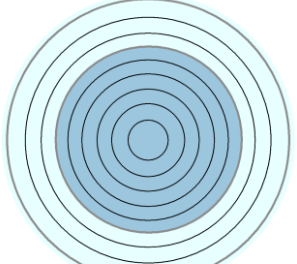
In the frame of ESFR-SMART project, EDF and PSI used the ERANOS code. Both organizations generated the respective 33-group cross sections by the ECCO module using the JEFF 3.1 based cross-section library with 1968 groups prepared for fast reactors. For all subcritical zones, the buckling used for spectrum modification was $0.98696E-2$, corresponding to a zone length of 25 cm. This value was determined in a separate study [15] and used as the most conservative value from the void reactivity perspective.

Full core models were based on VARIANT module for hexagonal-z 3D flux calculation. The EDF calculations were based on the input file generated by the SDDS optimization system used for defining the reference ESFR-SMART core design [16]. The PSI ERANOS calculations are based on the reactor specification and the input file is derived from the EDF input file.

Nonetheless, the EDF and PSI models differ in many aspects. For example, in the PSI case, some selected zones have special treatment and material definitions have the form required for EQL3D procedure and are often adopted directly from previous CP-ESFR core simulations rather than from the EDF input deck. The main difference, however, is related to the treatment of the structural materials. While EDF used homogeneous representation, in the PSI model, majority of radial zones are modelled in ECCO simulations as heterogeneous geometries respecting the reactor specification. The radial reflector assemblies and the control rod followers are also simulated as subcritical heterogeneous zones. However, there are two exceptions mentioned in Table 4. In these cases, the homogeneous simulation or the original heterogeneous geometry may cause problems: the first is the sodium plenum and the second is the control rods. In the first case, neutron streaming may occur in the voided plenum. To avoid an incorrect simulation, this zone could be simulated as homogeneous, or with original geometry but subdivided in many hexagonal segments, or as an equivalent cylinder corresponding to the original geometry. In the PSI model, the last option was selected (see Table 4). This way the resulting cross-section captured well the changes in the plenum void. In the case of control rods, the flat flux approximation used typically in ECCO simulation caused an overestimation in control rod worth. This is especially pronounced when a homogeneous model is used. Since it is not so easy to subdivide the complicated original heterogeneous geometry of the control rods into several segments, the equivalent cylindrical model was used. The geometries are illustrated in Table 4.

Compared to the homogeneous model, the cylindrical control rods absorption is less overestimated. In the upper parking position, the cylindrical model provides a slightly higher reactivity by tens of pcm. In the scrammed position, the impact is stronger and in the range of 100 pcm. Axial ERANOS model follows Fig. 2 excluding the foot and head regions.

Table 4. Illustration of equivalent cylindrical geometries used in the PSI ERANOS model including the indicative subdivision into concentric subzones

Geometry	Plenum	CSD rods	DSD rods
Exact			
Equivalent			

4. Results

This section presents and discusses the results of the fresh core neutronic calculations provided by the contributing organizations. The results are summarized in a table form (Table 5) and compared graphically in Figures 5 – 8. The CE-MC results obtained with Serpent (by HZDR) are considered as a reference for comparison purposes.

Table 5. Evaluated safety parameters, pcm units

	Code	ρ nominal	SCRAM	Sodium void reactivity					KD			
				Void1	Void2	Void3	Void4	Void5	KD1	KD2	KD3	KD4
HZDR	Serpent	3942	-4779	651	560	-704	-566	-329	-937	-902	-55	-64
CIEMAT	MCNP	4004	-4794	631	554	-685	-556	-346	-985	-942	-48	-51
JRC	MCNP	3919	-4839	625	575	-711	-564	-281	-888	-867	-25	-135
UPM	KENO	3918	-4785	638	570	-701	-569	-332	-888	-894	-52	-37
IRSN	MORET	3894	-4823	639	569	-755	-634	-448	-950	-959	-36	-93
NNL	WIMS	3991	-4633	690	603	-763	-616	-303	-1016	-980	-53	-54
PSI	ERANOS	3769	-5356	696	567	-734	-571	-287	-1040	-1008	-55	-58
EDF	ERANOS	3788	N/A	527	471	-684	-609	-485	-950	-910	-57	-56

Maximum reported standard deviation of reactivity (1σ) in pcm units: Serpent – 4; MCNP – 5; KENO – 4; MORET – 4.

4.1 Core reactivity and SCRAM

The core reactivity values are compared in Figure 5a and the differences relative to the Serpent reference are plotted in Figure 5b. In general, there is a reasonably good agreement between all contributors. The results obtained with all four MC codes, namely Serpent (HZDR), MCNP (CIEMAT, JRC), KENO (UPM) and MORET (IRSN), are very close and agree within about 60 pcm. The deterministic code WIMS (NNL) shows an excellent agreement of 50 pcm with the reference reactivity value. As compared to Serpent, deterministic results obtained with ERANOS/VARIANT by PSI and EDF underestimate the core reactivity by more than 200 pcm.

The SCRAM reactivity values are compared in Figure 6a and the differences relative to the Serpent reference are plotted in Figure 6b. As in the core reactivity case, Serpent, MCNP, KENO, and MORET show excellent agreement in SCRAM reactivity.

Concerning deterministic results, WIMS underestimates the SCRAM reactivity by about 150 pcm only. On the other hand, the ERANOS/VARIANT results obtained by PSI overestimate the SCRAM reactivity by more than 500 pcm. This issue can be partially attributed to the differences in the control rod modelling approaches employed by these organizations. For instance, PSI did not apply any equivalence procedure during the lattice calculations whereas an SPH-based equivalence was used in the WIMS calculation route. Indeed, early calculations performed by NNL using a homogenous representation of the CSD and DSD cells showed similar discrepancies, thus highlighting the importance of an equivalence procedure.

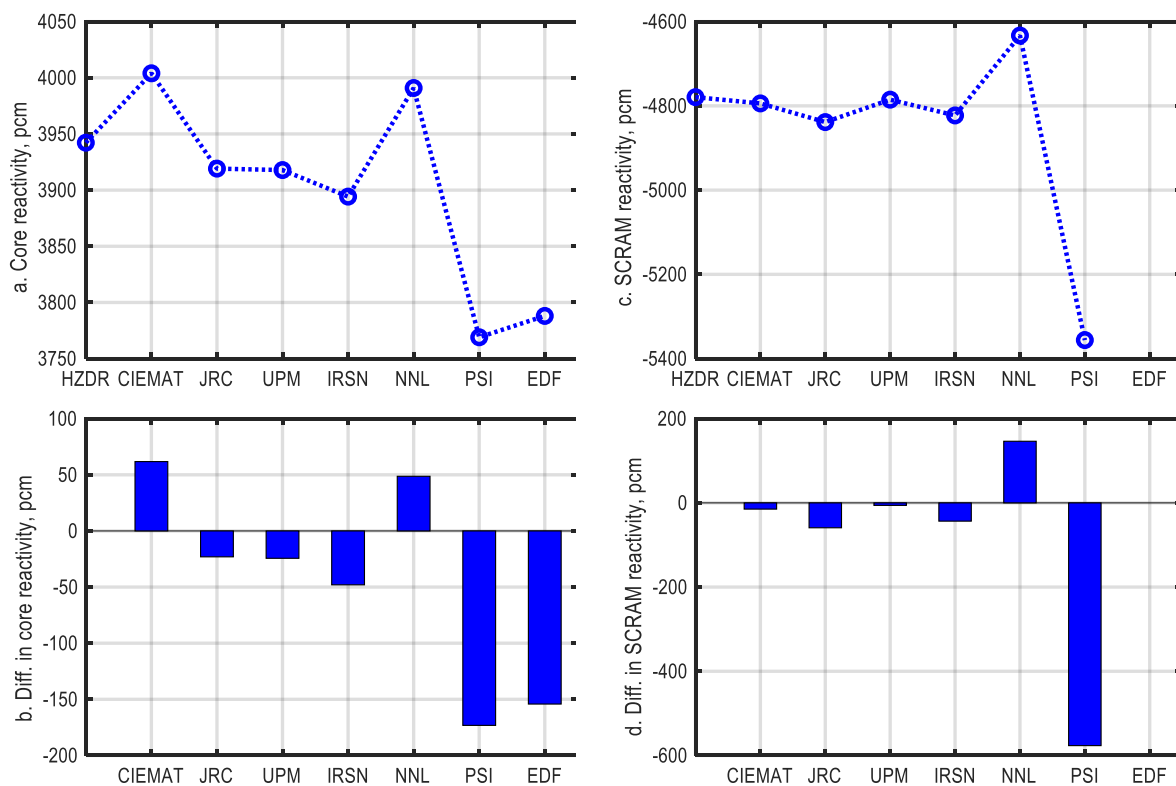


Fig. 5 Core and SCRAM reactivity

4.2 Sodium void reactivity

The sodium void reactivity values are compared in Figure 6 for the voiding scenarios Void 1-2 and in Figures 7 for the voiding scenarios Void 5 (cf. Figure 3).

The voiding of the inner and outer fissile zones (Void 1 and 2) results in a large positive reactivity effect (Figure 6a), as expected. The corresponding values produced by the MC codes Serpent, MCNP, KENO, and MORET agree reasonably well within a few percent. The deterministic WIMS, and ERANOS (PSI) results deviate to a somewhat higher extent from the reference. As can be seen from Figure 6b, there is a noticeable difference in the ERANOS results. On one hand, ERANOS (PSI) overestimates Void

1 by 7% and Void 2 by just 1%. On the other hand, ERANOS (EDF) shows an opposite trend and underestimates Void 1 and Void 2 by 17% and 19% respectively.

The Void 3 and Void 4 cases are related to the voiding of all regions above the inner and outer fissile zones. These voiding scenarios lead to a large negative reactivity effect (Figure 6c). As in the previous voiding scenarios, Serpent, MCNP, and KENO continue to exhibit a consistent mutual agreement (Figure 6d). Compared to Serpent, the MORET results overestimate the Void 3 and Void 4 values by 7% and 12% respectively, and WIMS by about 9% (Figure 6d). The ERANOS results produced by PSI show a good agreement with the reference while the difference in Void 3 and Void 4 is about 4% and 1% respectively. The EDF results show somewhat higher discrepancies of 3% and 8% for Void 3 and Void 4 respectively (Figure 6d).

The Void 5 case corresponds to the full core voiding. The resulting reactivity (Figure 7a) is a combination of two large effects acting in opposite directions, namely, a large positive effect due to the voiding of the fissile zones and large negative effect due to the voiding of the regions above. This case appears to be a more challenging scenario, in particular for the deterministic codes. Compared to the previous voiding scenarios, the Serpent and MCNP results show somewhat higher discrepancy while KENO is consistently close to Serpent (Figure 7b). MORET deviates by 36% from the reference value. The deterministic codes WIMS and ERANOS (PSI) underestimate the sodium void effect roughly by 10%. At the same time, ERANOS (EDF) overestimated the Void 5 value by about 50% (Figure 7b).

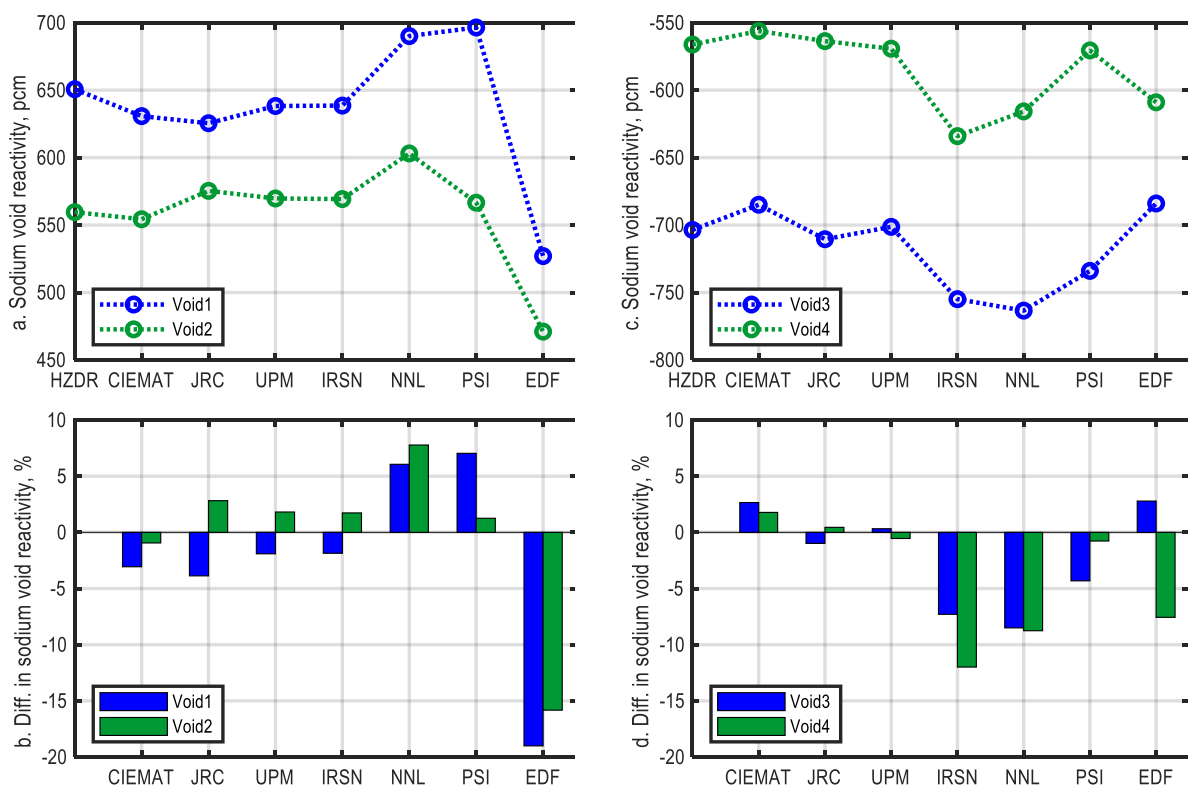


Fig. 6 Sodium void reactivity (Void 1, 2, 3 and 4)

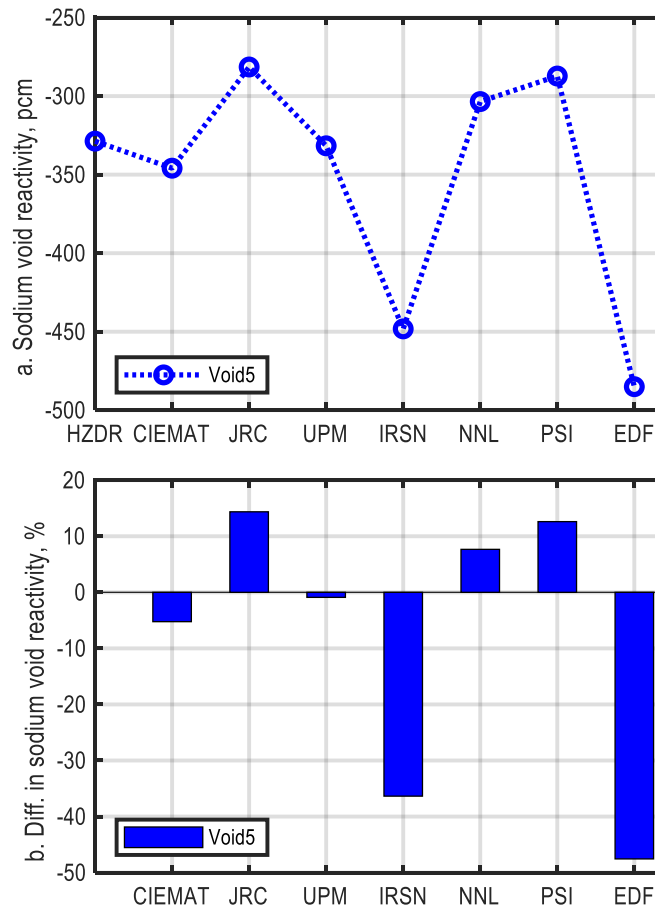


Fig. 7 Sodium void reactivity (Void 5)

4.3 Doppler constants

KD1 and KD2 are related to the reactivity effects due to the temperature variation of the inner and outer fissile regions respectively. The corresponding values are compared in Figure 8a and the differences relative to the Serpent reference are presented in Figure 8b.

The KD1 and KD2 values predicted by the MC codes MCNP, KENO, and MORET agree within 5% with those of Serpent. Surprisingly, the largest difference among the MC is between MCNP results produced by CIEMAT and JRC. As compared to the MC results, the deterministic codes predict somewhat higher Doppler effect, in particular WIMS and ERANOS (PSI), while ERANOS (EDF) is in good agreement with MC codes.

The KD3 and KD4 are related to the reactivity effects due to the temperature variation of the inner and outer fertile regions respectively. As the temperature variations of the fertile fuel have relatively low net reactivity effect, the results are rather inconclusive (Figure 8c). The ostensible large spread between the MC results for KD4 in Figure 8d is in terms of reactivity worth below 20 pcm. On the other hand, the deterministic codes agree with the reference within 4% for KD3 and 16% for KD4 (Figure 8d).

Due to the low neutronic importance of the fertile regions, the KD3 and KD4 values are more than an order of magnitude lower than KD1 and KD2. The absolute reactivity effect is about 20 pcm, which makes it challenging to obtain an accurate prediction by means of MC codes.

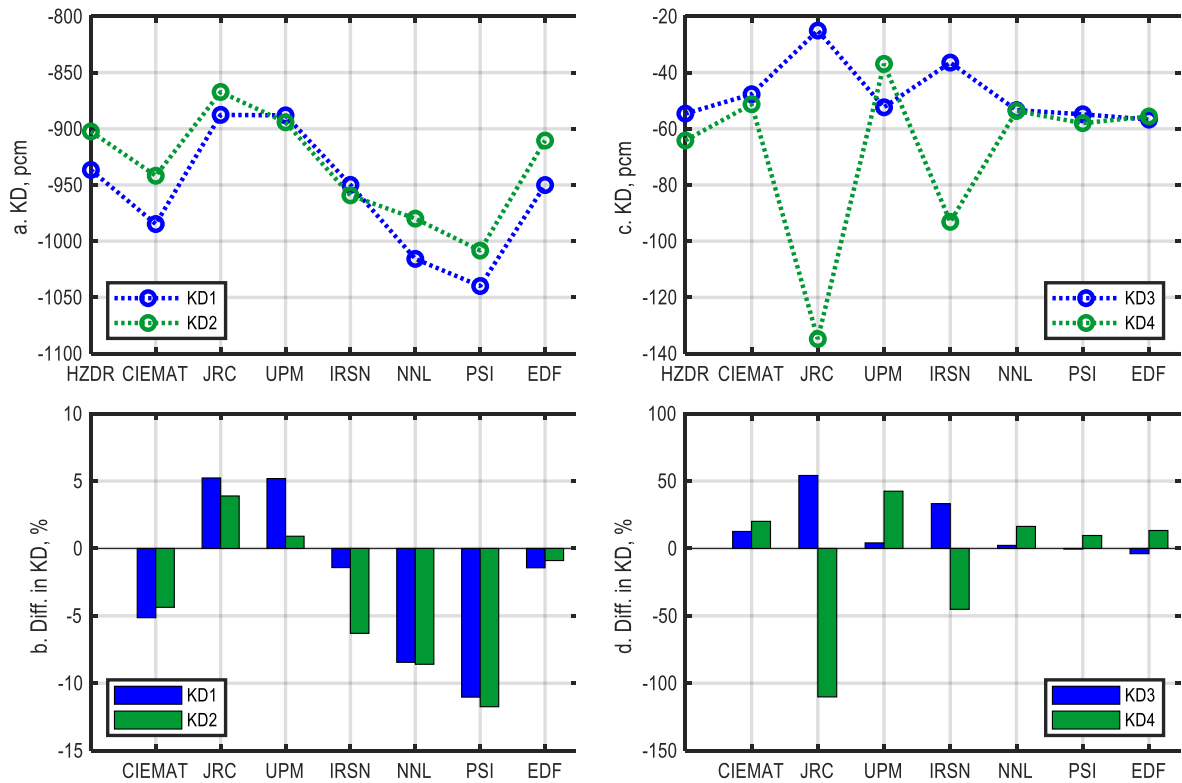


Fig. 8 Doppler constants

5. Summary and conclusions

In Part I of the paper, neutronic evaluation of the fresh ESFR core was performed. Parameters considered include core reactivity, SCRAM reactivity, sodium void reactivity for five different scenarios, as well as Doppler constants. These parameters were used to compare and tune the computational tools applied in the study. The outcome of the study can be summarized as follows.

The MC codes Serpent, MCNP, and KENO show consistently good mutual agreement practically in all considered parameters. Nevertheless, most of the observed differences exceed the reported statistical precision. This can be partially attributed to the differences in processing of the basic JEFF-3.1 library and preparation of the final cross section files utilized by the codes. This may include different cross section processing codes (i.e. NJOY [17] in case of Serpent and MCNP, and AMPX [18] in case of KENO), different versions of NJOY, reconstruction tolerance for pointwise cross sections in the resonance range, etc. As demonstrated in [19], Serpent and MCNP can agree on k -eff values within 1 pcm when using identical cross section files. The difference can rise to 100 pcm when differently processed cross sections are utilized by the codes.

The most problematic parameters are the KD3 and KD4 where the differences are noticeably higher. Temperature variations of the fertile fuel have relatively low net reactivity effect and, therefore, the results are rather sensitive to the MC statistics.

It is important to note that the preliminary results produced with KENO during the course of this study showed significantly worse agreement than Serpent and MCNP. In particular, KENO

systematically overestimated core reactivity by about 400-500 pcm as compared to other MC codes using the same library. In order to resolve this issue, a dedicated investigation was carried out. It was found out that the main reason for the observed discrepancies was incorrectly AMPX-generated probability tables for the unresolved resonance range. Therefore, the final KENO results were produced using the AMPX-formatted JEFF-3.1 library (processed at UPM) without employing the probability tables. A more detailed discussion and the major findings of the investigation can be found in [19].

It can be concluded that nuclear data are the main source of biases in MC simulations, ahead of the employed state-of-the-art MC code. Taking into account that a high credibility on the computational outcomes is required to make robust decisions based on simulations, the qualification of nuclear databases associated to MC codes is revealed to be a priority to support SFR development.

Regarding the MORET code, it shows good agreement with respect to the other Monte Carlo codes in nearly all considered parameters, except for the sodium void effect in the upper plenum, which is somewhat overestimated (and consequently so is the total void effect). This came as a surprise, as reactivity calculations carried out with the MORET code and other MC codes, on a large range of configurations, have always been in good agreement. Acceptable margins, when using well-matched conditions (model, data libraries, etc), have always been achieved. IRSN is looking into the issues in deep detail to understand and unveil the source of this inconsistency. Work is under way to investigate in particular the treatment of neutron scattering on Na at high energy.

One of the issues revealed in the course of this study is a noticeable difference between the PSI and EDF results obtained with ERANOS/VARIANT, which affects most of the major safety related parameters. A possible reason lies in the different treatment of non-multiplying media (plenum, reflectors, control rods, etc.) employed by the organizations: while PSI used heterogeneous models, EDF adopted a homogeneous representation of the non-multiplying media.

The initial core neutronic characterization will be followed by the once-through and multi-batch burnup analysis aimed at establishing the equilibrium core state. This, however, is a topic for Part II of the paper [5].

Funding

The research leading to these results has received funding from the Euratom research and training programme 2014-2018 under Grant Agreement Number 754501 (ESFR-SMART).

Acronyms and Abbreviations

3D - three-dimensional

CDT - corium discharge tubes

CE - continuous energy

ρ - reactivity

CSD - control and shutdown devices

DSD - diverse shutdown devices

ESFR - European Sodium Fast Reactor

ESFR-SMART - European Sodium Fast Reactor Safety Measures Assessment and Research Tools

IF - inner fuel

KD - Doppler constants

MC - Monte Carlo

MOC - method of characteristics

OF - outer fuel

pcm - per cent mille

SA - sub-assemblies

SPH - super-homogenization

References

- [1] Mikityuk K., Girardi E., Krepel J., Bubelis E., Fridman E., Rineiski A., Girault N., Payot F., Buligins L., Gerbeth G., Chauvin N., Latge C., Garnier J.-C., 2017. "ESFR-SMART: new Horizon-2020 project on SFR safety," in Proc. *IAEA FR2017*, Ekaterinburg, Russian Federation.
- [2] Fiorini G. L., Vasile A., 2011. "European Commission – 7th Framework Programme: The Collaborative Project on European Sodium Fast Reactor (CP ESFR)," *Nuclear Engineering and Design*, vol. 241, pp. 3461–3469.
- [3] Rineiski A., Meriot C., Marchetti M., Krepel J., Tsige-Tamirat H., Alvarez F., Girardi E., Mikityuk K., 2020. "New core safety measures and their preliminary assessment in the ESFR-SMART project," *Journal of Nuclear Engineering and Radiation Science*, (Submitted).
- [4] Rineiski A., Meriot C., Marchetti M., Krepel J., 2018. "Core Safety Measures in ESFR-SMART," in Proc. *PHYSOR 2018*, Cancun, Mexico.
- [5] Fridman E., Álvarez-Velarde F., Romojaro-Otero P., Tsige-Tamirat H., Jiménez-Carrascosa A., García-Herranz N., Bernard F., Gregg R., Davis U., Krepel J., Lindley B., Massara S., Pomerouly S., Girardi E., Mikityuk K., 2020. "Neutronic analysis of the European Sodium Fast Reactor: Part II - burnup analysis," *Journal of Nuclear Engineering and Radiation Science*, (Accepted), NERS-20-1067.

- [6] Koning A. J., Avrigeanu M., Avrigeanu V., Batistoni P., Bauge E., Bé M.-M., Bem P., Bernard D., Bersillon O., Bidaud A., Bouland O., Courcelle A., Dean C. J., Dos-Santos-Uzarralde P., Duchemin B., Duhamel I., Duijvestijn M. C., Dupont E., Fischer U., Forrest R. A., *et al.*, 2007. “The JEFF evaluated nuclear data project,” in Proc. *ND 2007*, Nice, France <https://doi.org/10.1051/ndata:07476>.
- [7] Leppänen J., Pusa M., Viitanen T., Valtavirta V., Kaltiaisenaho T., 2015. “The Serpent Monte Carlo code: Status, development and applications in 2013,” *Annals of Nuclear Energy*, vol. 82, pp. 142–150.
- [8] Pelowitz D. B., 2014. *MCNP6 User’s Manual, Code version 6.1.1beta*, LA-CP-14-00745, Los Alamos, NM, United States.
- [9] Goorley J. T., James M. R., Booth T. E., Bull J. S., Cox L. J., Durkee J. W. Jr., Elson J. S., Fensin M. L., Forster R. A. I., Hendricks J. S., Hughes H. G. I., Johns R. C., Kiedrowski B. C., Martz R. L., Mashnik S. G., McKinney G. W., Pelowitz D. B., Prael R. E., Sweezy J. E., Waters L. S., *et al.*, 2013. *Initial MCNP6 Release Overview - MCNP6 version 1.0*, Los Alamos NM, USA <https://doi.org/10.2172/1086758>.
- [10] Cochet B., Jinaphanh A., Heulers L., Jacquet O., 2015. “Capabilities overview of the MORET 5 Monte Carlo code,” *Annals of Nuclear Energy*, vol. 82, pp. 74–84.
- [11] Rearden B. T., Jessee M. A., 2017. *SCALE Code System*, 1800553684, ORNL/TM-2005/39, Oak Ridge National Laboratory, Oak Ridge, TN, United States <https://doi.org/10.2172/1408010>.
- [12] Lindley B., Hosking G., Smith P., Powney D., Tollit B., Fry T., Perry R., Ware T., Murphy C., Grove C., Thomas M., Hesketh K., Kotlyar D., 2017. “Developments within the WIMS Reactor Physics Code for Whole Core Calculations,” in Proc. *M&C 2017*, Jeju, South Korea.
- [13] Ruggieri J. M., Tommasi J., Lebrat J. F., Suteau C., Plisson-Rieunier D., De Saint Jean C., Rimpault G., Sublet J. C., 2006. “ERANOS 2.1: International code system for GEN IV fast reactor analysis,” in Proc. *ICAPP 2006*, Reno, Nevada, USA.
- [14] Kavenoky A., 1978. “The SPH Homogenization Method,” in Proc. *A Specialists’ Meeting on Homogenization Methods in Reactor Physics, IAEA-TECDOC-231*, Lugano, Switzerland.
- [15] Krepel J., Pelloni S., Bortot S., Panadero A. L., Mikityuk K., 2015. “Mapping of sodium void worth and doppler effect for sodium-cooled fast reactor - 15458,” in Proc. *ICAPP 2015*, Nice, France.
- [16] Rineiski A., Meriot C., Coquelet-Pascal C., Krepel J., Fridman E., 2018. *Specification of the new core safety measures*, H2020 ESRF-SMART, Project Deliverable D1.1.2(D1.2).
- [17] MacFarlane R. E., Kahler A. C., 2010. “Methods for Processing ENDF/B-VII with NJOY,” *Nuclear Data Sheets*, vol. 111, pp. 2739–2890.
- [18] Wiarda D., Dunn M. E., Green N. M., Williams M. L., Celik C., Petrie L. M., 2016. *AMPX-6: A Modular Code System for Processing ENDF/B evaluations*, ORNL/TM-2016/43, Oak Ridge, TN, United States.

- [19] Jiménez-Carrascosa A., Fridman E., García-Herranz N., Alvarez-Velarde F., Romojaro P., Bostelmann F., 2019. "About the impact of the Unresolved Resonance Region in Monte Carlo simulations of Sodium Fast Reactors," in Proc. *ICAPP 2019*, Nice, France <https://doi.org/10.5281/zenodo.3324476>.

